Bioactive Materials 50 (2025) 1–13

Contents lists available at ScienceDirect

Bioactive Materials

journal homepage: www.keaipublishing.com/en/journals/bioactive-materials

Mytilus edulis foot protein mimics for tailoring long-acting endothelium-mimicking anti-thrombotic surfaces

Zeyu Du [a,b], Yuting Huang [b], Qing Ma [a,b], Wentai Zhang [b], Yan Fu [b], Nan Huang [a,c], Xin Li [d,***], Zhilu Yang [a,b,**], Wenjie Tian [e,*]

[a] School of Materials Science and Engineering, Key Lab of Advanced Technology for Materials of Education Ministry, Southwest Jiaotong University, Chengdu, Sichuan, 610031, China
[b] Dongguan Key Laboratory of Smart Biomaterials and Regenerative Medicine, The Tenth Affiliated Hospital, Southern Medical University, Dongguan, Guangdong, 523059, China
[c] GuangZhou Nanchuang Mount Everest Company for Medical Science and Technology, Guangzhou, Guangdong, 510670, China
[d] Department of Cardiology, Affiliated Hospital of Southwest Jiaotong University, The Third People's Hospital of Chengdu, Chengdu, Sichuan, 610031, China
[e] Cardiology Department, Sichuan Provincial People's Hospital, University of Electronic Science and Technology of China, Chengdu, Sichuan, 610072, China

ARTICLE INFO

Keywords:
Mytilus edulis foot protein mimic
Chemical robustness
Endothelium mimicking
Long-acting antithrombosis
Anti-coagulant
Anti-platelet agent

ABSTRACT

Surfaces with enduring and superior antithrombotic properties are essential for long-term blood-contacting devices. While current surface engineering strategies integrating anticoagulants and antiplatelet agents show promise in mimicking the non-thrombogenic properties of the endothelium, their long-term effectiveness remains limited. Here, we report an easy-to-perform, dual-biomimetic surface engineering strategy for tailoring long-acting endothelium-mimicking anti-thrombotic surfaces. We first designed a *Mytilus edulis* foot protein-5 (Mefp-5) mimic rich in amine and clickable alkynyl groups to polymerize-deposit a chemical robust coating onto the surface through a mussel-inspired adhesion mechanism. Then, a clickable nitric oxide (NO, an anti-platelet agent)-generating enzyme and the anticoagulant heparin were sequentially co-grafted onto the chemical robust coatings via click chemistry and carbodiimide chemistry. Our results demonstrate that this engineered surface achieved an impressive NO catalytic release efficiency of up to 88 %, while heparin retained 86 % of its bioactivity even after one month of exposure to PBS containing NO donor. Both *in vitro* and *in vivo* experiments confirmed that this robust endothelium-mimicking coating substantially reduces thrombosis formation. Overall, our long-acting endothelium-mimicking anti-thrombotic coatings present a promising and feasible strategy to address thrombosis-related challenges associated with blood-contacting devices.

1. Introduction

Cardiovascular implantable biomedical devices (e.g., cardiac pacemakers, vascular stents, central venous catheters, and artificial hearts or valves) are widely used for medical monitoring, infusion, and disease treatment [1–5], significantly enhancing patients' quality of life. However, during clinical application, these long-term implants are inevitably prone to complications, such as coagulation and thrombosis, which can ultimately compromise their functionality [6,7]. In severe cases, such complications may lead to life-threatening events, or permanent disability [8–10]. To combat thrombosis, prolonged or lifelong administration of anticoagulants is commonly employed in clinical practice [11–13]. However, this strategy may inherently lead to side effects such as heparin-induced thrombocytopenia (HIT), bleeding, and increased liver burden [14–16].

The formation of thrombus on the surface of foreign materials is a well-established process involving two distinct yet interrelated events: (1) fibrin formation due to the activation of the coagulation cascade, and (2) platelet activation, adhesion, and aggregation mediated by a cyclic guanosine 3′,5′-monophosphate (cGMP)-dependent mechanism [17,18].

Peer review under the responsibility of editorial board of Bioactive Materials.
* Corresponding author.
** Corresponding author. School of Materials Science and Engineering, Key Lab of Advanced Technology for Materials of Education Ministry, Southwest Jiaotong University, Chengdu, Sichuan, 610031, China.
*** Corresponding author.
E-mail addresses: lixin@swjtu.edu.cn (X. Li), zhiluyang1029@swjtu.edu.cn (Z. Yang), tianwenjie@med.uestc.edu.cn (W. Tian).

https://doi.org/10.1016/j.bioactmat.2025.03.019
Received 6 March 2025; Received in revised form 22 March 2025; Accepted 23 March 2025
Available online 1 April 2025

Based on this understanding, numerous innovative surface engineering strategies have been explored to improve the blood compatibility of cardiovascular implants [19–21]. Among these, approaches that mimic the non-thrombogenic properties of the native endothelial cell (EC) layer lining the inner walls of blood vessels have shown the greatest promise [22–24]. The endothelium represents one of the best antithrombotic surfaces in nature, owing to the synergistic action of its secreted anti-platelet agents-NO and prostacyclin (PGI2)-along with key anticoagulants such as thrombomodulin (TM), tissue factor pathway inhibitor (TFPI), and heparan sulfates (structural analogs of heparin), which are localized at or near the luminal surface [25]. Over the past two decades, significant efforts have been devoted to replicating the highly thromboresistant properties of the natural endothelium by integrating anti-coagulant heparin and antiplatelet agent NO on the surfaces of blood-contacting materials/devices, with numerous studies reporting encouraging antithrombogenic performance and reproducing thrombomodulin-like responsiveness [26–28]. However, current technologies face challenges in sustaining long-acting anticoagulation functionality for long-term or permanently implanted cardiovascular devices. A main reason for the low persistence of the activity of these methods is seen in the adequate long-lasting immobilization of the anticoagulant heparin together with bioactive compounds capable of generating the antiplatelet agent NO on the surfaces of implants. Chemically robust coatings that overcome these two limitations bearing multiple reactive functional groups for covalent immobilizing anti-coagulant heparin and bioactive species capable of producing NO therefore represent a promising approach for long-lasting thromboresistance.

We present a biomimetic approach inspired by the mechanochemically robust adhesive plaques formed by *Mytilus edulis* foot proteins (Mefp), which are secreted by mussels for durable attachment to virtually all wet material surfaces [29]. It has been demonstrated that the mechanochemical robustness enables the mussel adhesive plaques to maintain strong and durable bonds with solid substrates, even under harsh conditions such as extreme acidity, alkalinity, and oxidative environments (Fig. 1A) [30]. Studies have identified Mefp-5 is a linear macromolecule enriched with multiple functional groups, where the coexistence of a flexible backbone and reactive moieties (i.e., catechol and amine groups) is essential for the strong and durable adhesion of mussel adhesive plaques to a wide range of materials (Fig. 1B and C) [31]. During the self-polymerization of Mefp-5, the catechol-amine synergism drives the formation of cross-linked, interpenetrating networks (Fig. 1D), endowing the adhesive plaque with unmatched chemical robustness [32].

Herein, inspired by the role of Mefp-5 in forming a robust adhesive plaque, we present a dual-biomimetic surface engineering strategy for tailoring long-acting endothelium-mimicking anti-thrombotic surfaces. Specifically, we synthesized a Mefp-5 mimic by co-modifying polyallylamine (PAm, Mw ~17 kDa) with 4-pentynoic acid (PA) and hydrogenated caffeic acid (HCA), resulting in an alkyne- and catechol-functionalized polyallylamine (ACPA, Fig. 1E). Leveraging the intrinsic catechol-polyamine synergy of ACPA, we fabricated a chemically robust polymeric pre-coating (PACPA, Fig. 1F) enriched with reactive primary amine groups and clickable alkynyl moieties on material/device surfaces. Subsequently, the clickable NO-generating copper chelator N_3-DOTA-Cu and heparin were sequentially co-grafted onto the PACPA using click chemistry and carbodiimide chemistry, resulting in a dual-functional endothelial-mimetic anti-thrombotic surface (Fig. 1G). Benefiting from the chemical robustness and the capability of PACPA for tethering biomolecules, the endothelium-mimicking coating exhibits exceptional chemical robustness even under harsh conditions (HCl (pH 2), NaOH (pH 13), and H_2O_2 (0.3 % w/w)), ensuring long-term retention (>86 % bioactivity after 4 weeks) of both immobilized biomolecules even after 4 weeks of immersion in simulated physiological fluids. This robust bioactivity retention endows the coating with long-lasting endothelium-like antithrombotic properties, effectively inhibiting platelet activation through sustained NO release, synergistic with heparin-mediated coagulation factor inactivation, thereby ensuring long-term anti-thrombotic efficacy (Fig. 1H). Overall, our findings highlight a promising strategy for engineering durable and highly effective antithrombotic surfaces for blood-contacting materials and medical devices.

2. Materials and methods

2.1. Materials

Polyallylamine solution (PAm, Mw ~17,000, 20 wt% in H_2O), 3,4-dihydroxy hydrocinnamic acid (HCA, purity ≥97.0 %), 4-Pentynoic acid (PA, purity ≥95.0 %), Azido-mono-amide-DOTA (N_3-DOTA, purity ≥85.0 %), Heparin sodium (Heparin, ≥99 %), S-nitrosoglutathione (GSNO, purity ≥97.0 %), N-(3-dimethylaminopropyl)-N′-ethyl-carbodiimide (EDC, purity ≥98.0 %), N-hydroxysuccinimide (NHS, purity ≥97.0 %), 2-(N-morpholino) ethanesulfonic acid hydrate (MES, purity ≥99 %), $CuSO_4{\cdot}5H_2O$ (≥99.0 %), Sodium ascorbate (≥99.0 %), N,N-Diisopropylethylamine (DIPEA, ≥99.0 %), Fibrinogen (Fg ≥ 85.0 %), Human serum albumin (HSA, ≥96.0 %), Immunoglobulin G (IgG, ≥95.0 %), and L-glutathione (GSH, purity ≥97.0 %) were purchased from Sigma-Aldrich (Shanghai, China). Deionized water (DI, 18.2 MΩ cm^{-1}), Sodium hydroxide (NaOH, purity ≥98.0 %), Acid Orange II (purity ≥96.0 %), Phosphate buffer solution (PBS, 10 mM), Copper chloride dehydrate ($CuCl_2{\cdot}2H_2O$), Hydrogen peroxide solution (H_2O_2, 0.3 % (w/w)), and Hydrochloric acid (HCl) were purchased from Aladdin Reagent (Shanghai, China). Chromogenix Factor IIa (FIIa) and Factor Xa (FXa) kits (Chromogenix Coamatic® Heparin) were purchased from Chromogenix Co., Ltd. (Milano, Italy). Activated partial thromboplastin time (APTT) was purchased from Beyotime Biotechnology Co., Ltd. (Shanghai, China). cGMP ELISA kit was purchased from Wuhan MSK Biotechnology Co., Ltd. (Wuhan, China). 316L stainless steel (SS) was purchased from Corsair Medical Technology Co., Ltd. (Suzhou, China). New Zealand white rabbits were purchased from Shanghai Model Organisms Center, Inc.

2.2. Synthesis of ACPA and N_3-DOTA-Cu

ACPA was synthesized using standard EDC/NHS chemistry. To prevent the oxidation of the catechol groups in HCA, the MES buffer (pH 5.6) was first deoxygenated with high-purity nitrogen for 2 h. Subsequently, HCA (100 mg mL^{-1}), PA (200 mg mL^{-1}), EDC (800 mg mL^{-1}), and NHS (200 mg mL^{-1}) were dissolved in 100 mL of the deoxygenated MES buffer and activated at 37 °C for 30 min. PAm (1 mg mL^{-1}) was then introduced into the reaction mixture, followed by continuous stirring at 10 °C for 24 h. The crude product was purified through dialysis (molecular weight cutoff: 1000 Da) against deoxygenated DI for 48 h, with water replacement every 6 h, and lyophilized to obtain the final ACPA.

For the NO-generating complex, the N_3-DOTA-Cu coordination compound was prepared by reacting N_3-DOTA (1 mg mL^{-1}) with $CuCl_2{\cdot}2H_2O$ (0.35 mg mL^{-1}) in aqueous solution at room temperature for 15 min, ensuring the complete chelation of Cu^{2+} ions.

2.3. Structural characterization

The chemical structures of HCA, PA, PAm and ACPA were characterized using a ^{1}H nuclear magnetic resonance (^{1}H NMR) spectrometer (Bruker Avance III 400 MHz spectrometer, Germany) and Fourier transform infrared (FTIR) spectroscopy (Nicolet 5700, Thermo Fisher Scientific, USA). Electron paramagnetic resonance (EPR) spectroscopy (A320, Bruker, Germany) was employed to analyze the coordination structure of the N_3-DOTA-Cu complexes.

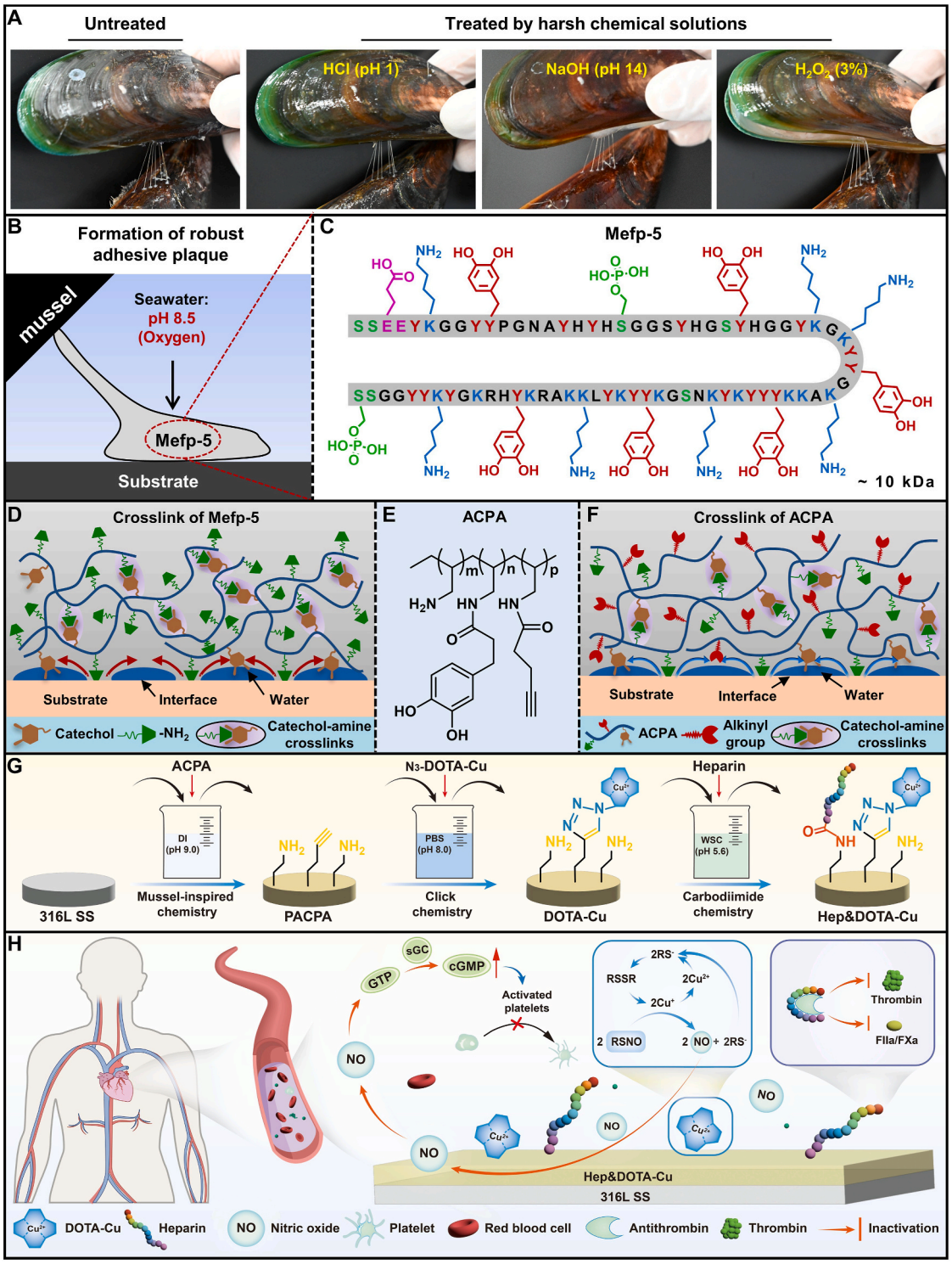

Fig. 1. The development of enduring and highly anti-thrombotic surfaces for long-term blood-contacting devices, inspired by the role of Mefp-5 in forming robust adhesive plaques, the integration of heparin as an anti-coagulant and NO as an anti-platelet agent, to mimic the non-thrombogenic properties of the natural endothelium. (A) The abilities of mussel adhesive plaque to resist chemical corrosion of harsh chemical solutions including strong acid (HCl, pH 1), base (NaOH, pH 14), and oxidant (H_2O_2, 3 % (w/w)). (B) Schematic illustrations of Mefp-5 in the formation of robust adhesive plaques and (C) the amino acid sequence of Mefp-5 [33]. (D) Schematic illustration of the interfacial location and chemical crosslink of Mefp-5 to form a robust adhesive plaque on the substrate through phenol-polyamine synergy. (E) The synthetic Mefp-5-like alkyne- and catechol-functionalized polyallylamine (ACPA) mimics not only the role of multiple functional groups but also the macromolecular backbone of Mefp-5 in the formation of highly adhesive, robust adhesive plaque. (F) Schematic representation of adhesion, crosslinking, and progressive assembly of ACPA as a macromolecular building block to form the highly adhesive, robust, multifunctional PACPA coatings on substrates based on phenol-polyamine synergy. (G) Illustration of the preparation process of the long-acting endothelium-mimicking antithrombotic coatings on substrates. (H) Schematic depiction of the developed dual-biomimetic antithrombotic coatings to closely mimic the anti-thrombotic function of natural endothelium via the anti-coagulant heparin and anti-platelet NO working synergistically at the blood/substrate interface.

2.4. Preparation of the PACPA coating

The ACPA was dissolved in deoxygenated DI (1 mg mL^{-1}), and 316L SS was immersed in the solution. The pH was adjusted to 9 using NaOH, and the reaction was carried out at 37 °C for 24 h under micro-oxygenated conditions. This process was repeated 3 times to achieve a dense and uniform PACPA coating.

2.5. Click chemistry-mediated immobilization of N_3-DOTA-Cu

N_3-DOTA-Cu (1 mg mL^{-1}), copper sulfate pentahydrate (6.5 mg mL^{-1}), and sodium ascorbate (10 mg mL^{-1}) were dissolved in PBS buffer (pH 7.4), respectively. The three solutions were then mixed at a volume ratio of 20:1:1, and DIPEA was added to the mixture to adjust the pH to 8.0. Subsequently, the reaction was performed at room temperature in the dark for 12 h. Afterward, the resulting product was washed thoroughly with DI and dried using N_2 gas. Finally, DOTA-Cu-PACPA with NO catalytic activity was obtained (marked as DOTA-Cu).

2.6. Sequential co-immobilization of heparin

Heparin was covalently grafted onto the surface using water-soluble carbodiimide (WSC) chemistry. Briefly, heparin (1 mg mL^{-1}) was dissolved in MES buffer (pH 5.6) containing EDC (3 mg mL^{-1}), followed by activation at 37 °C for 30 min. Subsequently, 1 mL of the heparin solution was dropwise added onto the PACPA- or DOTA-Cu-coated surface and allowed to react at 37 °C for 24 h. Finally, the surface was ultrasonically cleaned with DI and dried with N_2, to obtain the heparin-functionalized coating (labeled as Hep or Hep&DOTA-Cu).

2.7. Characterizations

The water contact angle (WCA) was determined by a KrüssGmbH DSA 100 Mk 2 goniometer (Hamburg, Germany). The chemical components of the coatings were identified by X-ray photoelectron spectroscopy (XPS, AXIS Supra, Kratos Analytical Inc., Japan) equipped with a monochromatic A1 Kα (1468.6 eV) X-ray source operated at 12 kV and 15 mA at a pressure of 3×10^{-7} Pa. The C1s peak (284.8 eV) was used for charge calibration. The thickness of these coatings was investigated by a spectroscopic ellipsometer (W-VASE, J.A. Woollam, USA). Surface morphology and roughness were characterized using scanning electron microscopy (SEM, JSM-7001F, Japan), and 3D profilometry (VK-X3000, Keyence, Japan). The optical density (OD) values of eluates from the coatings were detected at 480 nm with a microplate reader (Biotek, USA).

2.8. Quantification of amine groups

The amine group density on the surfaces was measured using the acid orange II. First, 100 μL of acid orange II solution (3.5 mM, pH 3) was added to the surface of each sample and incubated at 37 °C for 12 h. Following the reaction, the samples were rinsed with HCl (pH 3) to remove unbound acid orange II and then dried with N_2. Subsequently, 200 μL of NaOH solution (pH 12) was added to the surface and incubated at 37 °C for 15 min. Finally, the concentration of acid orange II released into the NaOH solution was measured at 485 nm using a microplate reader (μQuant, Bio-Tek Instruments Inc.). A standard curve for amine group quantification was established by measuring the adsorption density of acid orange II across a series of concentration gradients.

2.9. Assessment of the chemical robustness of mussel adhesive plaques and PACPA

To evaluate the chemical robustness of mussel adhesive plaques, they were treated with extreme solutions (HCl (pH 1), NaOH (pH 14), and H_2O_2 3 % (w/w)) for 6 h, and their resistance to chemical erosion was evaluated by checking morphological changes.

The chemical robustness of the PACPA and Hep&DOTA-Cu coatings was evaluated by immersing the samples in solutions with HCl (pH 2), NaOH (pH 13), or H_2O_2 (0.3 % w/w)) at 37 °C for 24 h. Following the incubation, the absorbance of the eluate, surface morphology, WCA, film thickness, surface roughness, and chemical composition of the coatings were analyzed using spectral photometry, SEM, spectroscopic ellipsometry, and XPS, respectively. To assess the long-term chemical robustness of the Hep&DOTA-Cu surface, samples were immersed in PBS solution at 37 °C for 7 (week 1), 14 (week 2), and 28 days (week 4), with an additional 10 μL of NO donor (10 μM GSNO/GSH) supplemented. At the designated time points, samples were collected and assessed for their elemental composition, NO catalytic efficiency, and anticoagulant properties.

2.10. Quantification of N_3-DOTA-Cu bound to the PACPA coatings

Real-time quantification of N_3-DOTA-Cu bound to PACPA coatings was performed using a quartz crystal microbalance with dissipation (QCM-D, Q-sense AB, Biolin Scientific, Sweden). The PACPA coatings were applied to Au-coated quartz crystals, which were then mounted in the QCM-D reaction chamber for analysis. First, a PBS buffer containing copper sulfate pentahydrate, sodium ascorbate, and DIPEA was injected into the chamber at a flow rate of 50 μL min^{-1} until the QCM signal stabilized, establishing a baseline. Then, the N_3-DOTA-Cu was dissolved in PBS with copper sulfate pentahydrate, sodium ascorbate, and DIPEA, and introduced into the chamber at the same flow rate. The reaction was allowed to proceed until equilibrium was achieved. Finally, unbound N_3-DOTA-Cu was rinsed off using PBS, and the amount of bound N_3-DOTA-Cu was determined based on the change in the QCM signal.

2.11. Quantification of heparin bound to the PACPA coatings

Real-time quantification of surface-immobilized heparin was performed using a QCM-D. PACPA coatings were applied to Au-coated quartz crystals, which were then placed in the reaction chamber for analysis. Initially, MES buffer solution (pH 5.6) was injected into the chamber at a flow rate of 50 μL min^{-1} until a stable QCM baseline was achieved. Subsequently, heparin, dissolved in MES buffer containing EDC and NHS, was introduced into the chamber at the same flow rate until the QCM signal equilibrated. Finally, unbound heparin was rinsed with PBS.

2.12. Catalytic release of NO

The catalytic NO release from different surfaces was measured using a chemiluminescence nitric oxide analyzer (NOA, Sievers 280i, Boulder, CO). Briefly, samples were placed in a reaction chamber containing 5 mL PBS, with 50 μL of NO donor (10 μM GSNO/GSH). The NO released from the surface was transported via a N_2 stream through the reaction chamber to the NO analyzer. The amount of NO was quantified using a pre-established calibration curve, as detailed in the literature [34].

2.13. Blood collection

Fresh whole blood was collected from New Zealand white rabbits in accordance with strict ethical standards and following the 3R Principle of the Animal Protection Act, with trisodium citrate anticoagulant added at a ratio of 9:1 (v/v). The blood was centrifuged at 3500 rpm or 1500 rpm for 15 min to obtain platelet-poor plasma (PPP) or platelet-rich plasma (PRP), respectively.

2.14. Hemolysis test

For the hemolysis test, fresh citrate anticoagulated rabbit whole blood was diluted with saline at a 4:5 (v/v) ratio to prepare diluted

blood. Test samples were placed in 9.8 mL saline, with 9.8 mL of saline and DI as the negative and positive controls, respectively. All samples were incubated at 37 °C for 30 min. Subsequently, 0.2 mL of the diluted blood was added to each sample, and the mixtures were incubated at 37 °C for another 1 h and centrifuged at 3000 rpm for 5 min. Finally, 200 μL of the supernatant was collected to measure the absorbance at 540 nm. The hemolysis rate (R) was calculated using the following formula:

$$(R) = \frac{(A - C1)}{(C2 - C1)} \times 100\% \quad (1)$$

Where *R* is the hemolysis rate, *A* is the absorbance of the test sample, *C1* is the absorbance of the negative control, and *C2* is the absorbance of the positive control.

2.15. In vitro whole-blood evaluation

A total of 200 μL of anticoagulant-free rabbit whole blood was applied dropwise to the surface of each sample (1 × 1 cm). After 5 min of static incubation at 37 °C, the samples were tilted to a 90° vertical orientation to simulate physiological shear conditions, and the blood flow behavior was recorded. Samples were then gently rinsed with PBS (pH 7.4) to remove non-adherent blood components and fixed in 2.5 wt % glutaraldehyde for 24 h at 4 °C. Thrombus morphology and platelet adhesion were analyzed using SEM.

2.16. Clotting time, FIIa and FXa activity

To measure APTT, the samples were placed in a 24-well plate and incubated with 350 μL of fresh rabbit PPP at 37 °C for 30 min. APTT reagent was added, and clotting time was measured using a coagulometer following the manufacturer's protocol.

The activities of FIIa and FXa on different sample surfaces were evaluated using respective chromogenic assay kits. The procedure involved adding 50 μL of PPP to the sample surfaces and incubating at 37 °C for 30 min. All steps were carried out according to the chromogenic assay kit manual.

To assess sustained anticoagulant functionality, samples were incubated in 2 mL PBS (pH 7.4) at 37 °C on a shaker for durations of 7, 14, and 28 days, with daily PBS replacement. At each time point, NO release (via chemiluminescence), Anti-FIIa, and -FXa activities were evaluated as described above.

2.17. Protein adsorption

Protein adsorption on the functionalized surfaces was quantified using QCM-D in real time. Briefly, gold-coated quartz chips coated with PACPA, DOTA-Cu, Hep, and Hep&DOTA-Cu were placed in the QCM-D reaction chamber. PBS buffer (pH 5.6) was injected at a flow rate of 50 μL min^{-1} until the quartz chip frequency stabilized. Subsequently, PBS solutions containing 2 mg mL^{-1} of HSA, Fg, or IgG were introduced into the chamber, and frequency changes were monitored. After stabilization, unbound proteins were rinsed by PBS rinsing, and stable adsorption was confirmed by post-rinse signal stabilization.

2.18. Platelet adhesion activation, and cGMP quantification

To assess platelet adhesion and activation on various samples surfaces, 200 μL of PRP was added dropwise onto the surfaces of different samples and incubated at 37 °C for 30 min, with an additional 10 μL of NO donor (10 μM GSNO/GSH). After incubation, the surfaces were rinsed 5 times with PBS and fixed overnight in 2.5 wt% glutaraldehyde solution. The samples were subsequently dehydrated using a graded ethanol series, dried, and examined via SEM, as detailed in the literature [35].

The expression levels of cGMP in platelets adhered to different surfaces were determined using ELISA kits. First, 1 mL of PRP was added dropwise to each sample surface and incubated at 37 °C for 30 min. Subsequently, the platelets were lysed with 0.1 % (v/v) Triton X-100 and ultrasonicated for 1 min, followed by centrifugation (2500 rpm, 5 min). Finally, the collected supernatant was then used for cGMP quantification, with cGMP levels measured following the manufacturer's protocol.

2.19. Ex vivo thrombogenicity assessment

In this study, a total of 18 male New Zealand white rabbits (2.5–3.0 kg) were used, and all were euthanized after the experiment. The rabbits were anesthetized via intravenous injection of sodium pentobarbital solution (30 mg kg^{-1}) through the marginal ear vein. The right carotid artery and left jugular vein were then surgically exposed. Subsequently, NO donor (10 μM GSNO/GSH, 0.1 mL kg^{-1}) was injected into the rabbits. The samples (1.5 × 0.9 cm) were curled inside a medical-grade three-way PVC catheter, which was then connected to the exposed artery and vein to establish an arteriovenous extracorporeal circulation. After 2 h of extracorporeal circulation, the catheters were collected and photo documented. The foils were taken out, weighed, photographed, and fixed with 2.5 % glutaraldehyde for SEM observation.

2.20. Statistical analysis

All data are presented as the mean ± standard deviation (SD). Each experiment was repeated three times independently. Statistical significance was assessed using one-way ANOVA, followed by Tukey's multiple comparison test to analyze differences among groups. An independent samples *t*-test was used to compare two groups, with $p < 0.05$ suggesting a significant difference.

3. Results and discussion

3.1. Fabrication and characterization of PACPA coating

The synthesis of the Mefp-5 mimic ACPA was conducted using carbodiimide chemistry, enabling the formation of amide bonds between the carboxyl groups of PA and HCA and the primary amine groups of PAm (Fig. 2A). To prevent oxidation of the hydroxyl groups in HCA, the reaction was conducted in an acidic (pH 5.6) and oxygen-free environment. The purified ACPA was characterized using ^{1}H NMR and FTIR spectroscopy. In the ^{1}H NMR spectrum, ACPA exhibited distinct signals corresponding to the aromatic protons of HCA (aromatic ring proton, δ6.94), the alkyne protons of PA (≡CH,δ2.67), and the acetyl group of PAm (-$COCH_3$, δ1.82), confirming the successful conjugation of HCA and PA with PAm (Fig. 2B). FTIR analysis further validated the successful synthesis of ACPA, as evidenced by the characteristic absorption peaks at 3468 cm^{-1} and 1604 cm^{-1}, corresponding to the -OH and aromatic -C=C- stretching vibrations of HCA in ACPA [36]. Additionally, the absorption peaks at 3280 cm^{-1} and 2115 cm^{-1} were attributed to the ≡ C-H and -C ≡ C- stretching vibrations of PA [37,38]. The stretching vibrations of -NH_2 and -CH_2 associated with the PAm functional group are prominently enhanced at 3362 cm^{-1} and 2926 cm^{-1} [39], respectively. Furthermore, the enhanced amide I and II bands at 1640 cm^{-1} and 1550 cm^{-1} further confirmed the successful co-modification of PAm with HCA and PA (Fig. 2C) [40]. Overall, these results confirm the successful synthesis of ACPA, which is enriched with reactive amine groups and clickable alkyne functional groups.

Subsequently, the feasibility of the synthesized ACPA to form chemically robust pre-coating (PACPA) was evaluated (Fig. 2D). Given its excellent chemical stability and mechanical properties, 316L SS is widely used in interventional therapies, making it an ideal substrate for further investigation [41,42]. The PACPA-modified surface exhibited a pale-yellow color compared to the bare 316L SS, confirming the

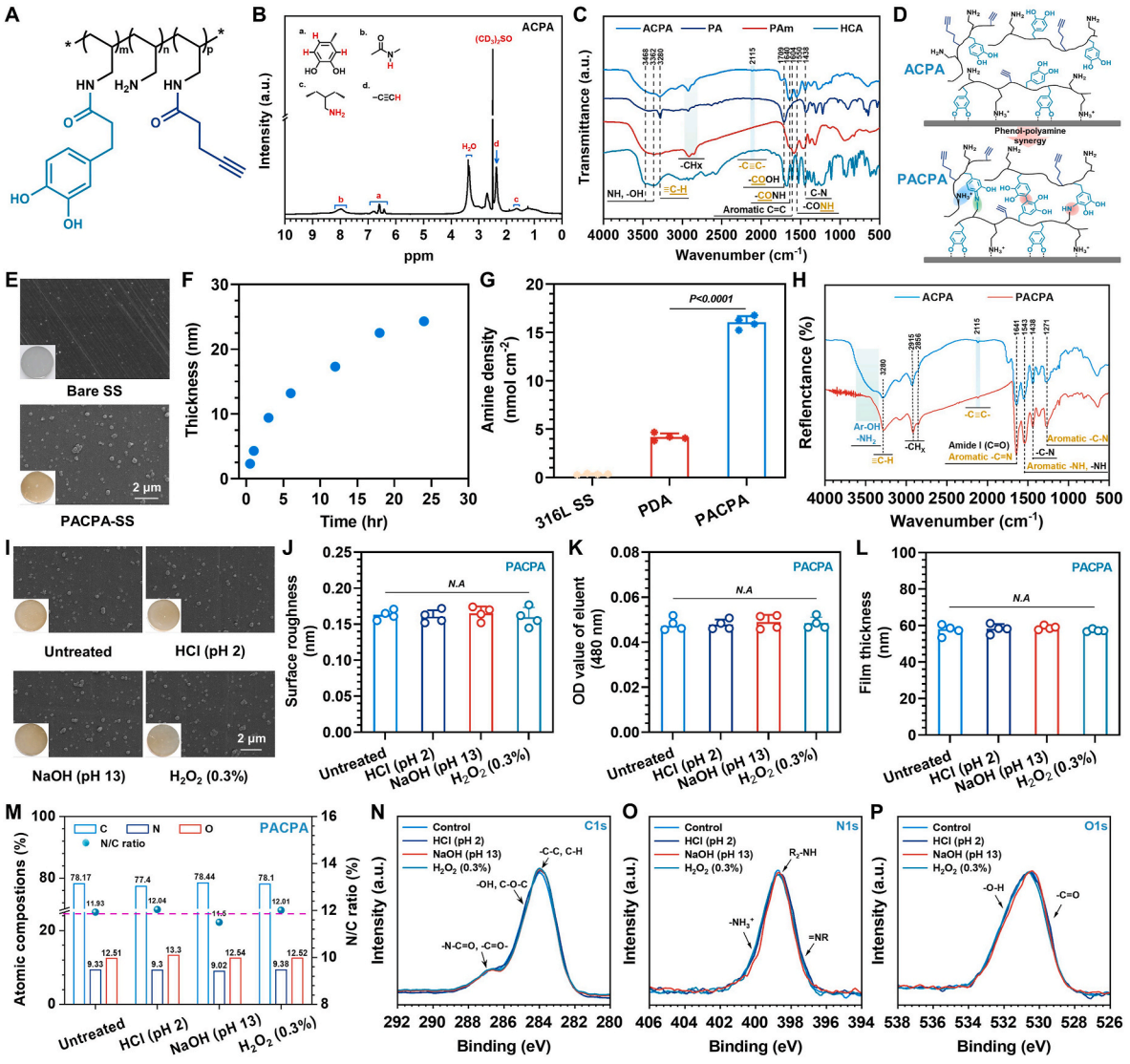

Fig. 2. Synthesis of ACPA and preparation and characterization of PACPA coatings. (A) Chemical structure of ACPA. (B) ^{1}H NMR spectrum of ACPA. (C) FTIR spectra of HCA, PA, PAm, and ACPA. (D) Schematic representation of ACPA forming a PACPA coating on a substrate through phenol-polyamine synergy. (E) Macroscopic images and SEM micrographs of 316L SS before and after PACPA coating. (F) Time-dependent variation in PACPA coating thickness on the substrate surface. (G) Surface amine group density on 316L SS, PDA, and PACPA coatings. (H) FTIR spectra of ACPA before and after polymerization (PACPA). (I) Macroscopic images and SEM micrographs of PACPA coatings before and after 24 h exposure to harsh environments (pH 2, pH 13, and H_2O_2, 0.3 % (w/w)). (J) Surface roughness of PACPA coatings before and after 24 h treatment in harsh environments. (K) The OD values (480 nm) of the solutions containing PACPA-coated 316L SS after 24 h of exposure to harsh environments (pH 2, pH 13, and H_2O_2 0.3 % (w/w)). (L) The film thickness and (M) atomic compositions (%) of PACPA coatings before and after 24 h exposure to harsh environments (pH 2, pH 13, and H_2O_2 0.3 % (w/w)). High-resolution spectra of C1s (N), N1s (O), and O1s (P) of PACPA coatings before and after treatment in harsh environments. One-way ANOVA followed by Tukey's multiple comparison test was performed to determine the *p*-values as indicated, and $p < 0.05$ suggests a significant difference. *"N.A"* indicates no significant differences between groups. All error bars represent the mean ± SD ($n = 4$).

successful fabrication of the PACPA coating. The 316L SS substrates were completely covered by the PACPA coating (Fig. 2E and S1), suggesting that the PACPA coating was dense and uniform. Further analysis revealed that the thickness of the PACPA coating increased with the oxidation time of ACPA (Fig. 2F), implying that the coating was formed through progressive oxidative cross-linking polymerization. Additionally, the surface of PACPA exhibited a high density of active grafting sites, with a primary amine group density of 16.04 ± 0.65 nmol cm^{-2}, which is three times higher than that of dopamine-based coatings (Fig. 2G). This high-density surface provides a promising foundation for robustly anchoring of sufficient biomolecule doses.

To further elucidate the formation mechanism of PACPA coating, the chemical structures of ACPA before and after oxidation were characterized using FTIR and XPS. As shown in Fig. 2H, the enhancement of Ar-C=N at 1641 cm^{-1} and the decrease of aromatic Ar-OH at 3400 cm^{-1} suggest that Ar-OH undergoes oxidation during PACPA formation and participates in Schiff base reactions with -NH_2, facilitating crosslinking polymerization [43]. Furthermore, XPS analysis confirmed that ACPA polymerization was primarily achieved through catechol-amine chemical crosslinking, mainly involving Michael addition and Schiff base reactions between the amine and catechol groups of ACPA [44] (Fig. S2).

Considering the critical role of chemical robustness in maintaining the enduring biological functionality of the coatings [45,46], we evaluated the stability of PACPA coatings under extreme conditions (pH 2, pH 13, and H_2O_2 0.3 % (w/w)). As shown in Fig. 2I, after exposure to these extreme conditions, the PACPA-coated 316L SS exhibited no noticeable changes in color and morphology, indicating that the coatings remained firmly adherent to the substrate without damage or peeling. The consistent surface roughness further supported this result (Fig. 2J). Moreover, the OD_{480}-values of the immersion solutions

remained unchanged (Fig. 2K), demonstrating that the PACPA coating did not dissolve or degrade [30]. Similarly, the film thickness of the coating remained consistent before and after treatment (Fig. 2L), confirming the preservation of the structural integrity. Notably, XPS analysis revealed no significant changes in the elemental content or chemical composition of the PACPA coatings before and after exposure to extreme conditions, further validating their exceptional chemical robustness (Fig. 2M–P and S3). These findings strongly support the excellent chemical robustness of PACPA coatings under harsh chemical environments, which is crucial for maintaining long-term biomolecular activity.

3.2. Fabrication of endothelium-mimicking antithrombotic surfaces

The long-term and highly effective antithrombotic performance of blood-contacting device surfaces is strongly influenced by the grafting type, density, and stable anchorage of biomolecules [39]. By leveraging the abundant alkynyl and amine groups in the PACPA coating, the grafting efficiency and biological effects of NO-generating enzyme (N_3-DOTA-Cu) and heparin were systematically investigated (Fig. 3A). First, the EPR spectrum of N_3-DOTA-Cu displayed a signal in the range of 3490-3430 mT, confirming the successful chelation of Cu^{2+} to N_3-DOTA [47] (Fig. S4). Subsequently, real-time QCM-D monitoring of mass changes during the grafting process showed that N_3-DOTA-Cu was

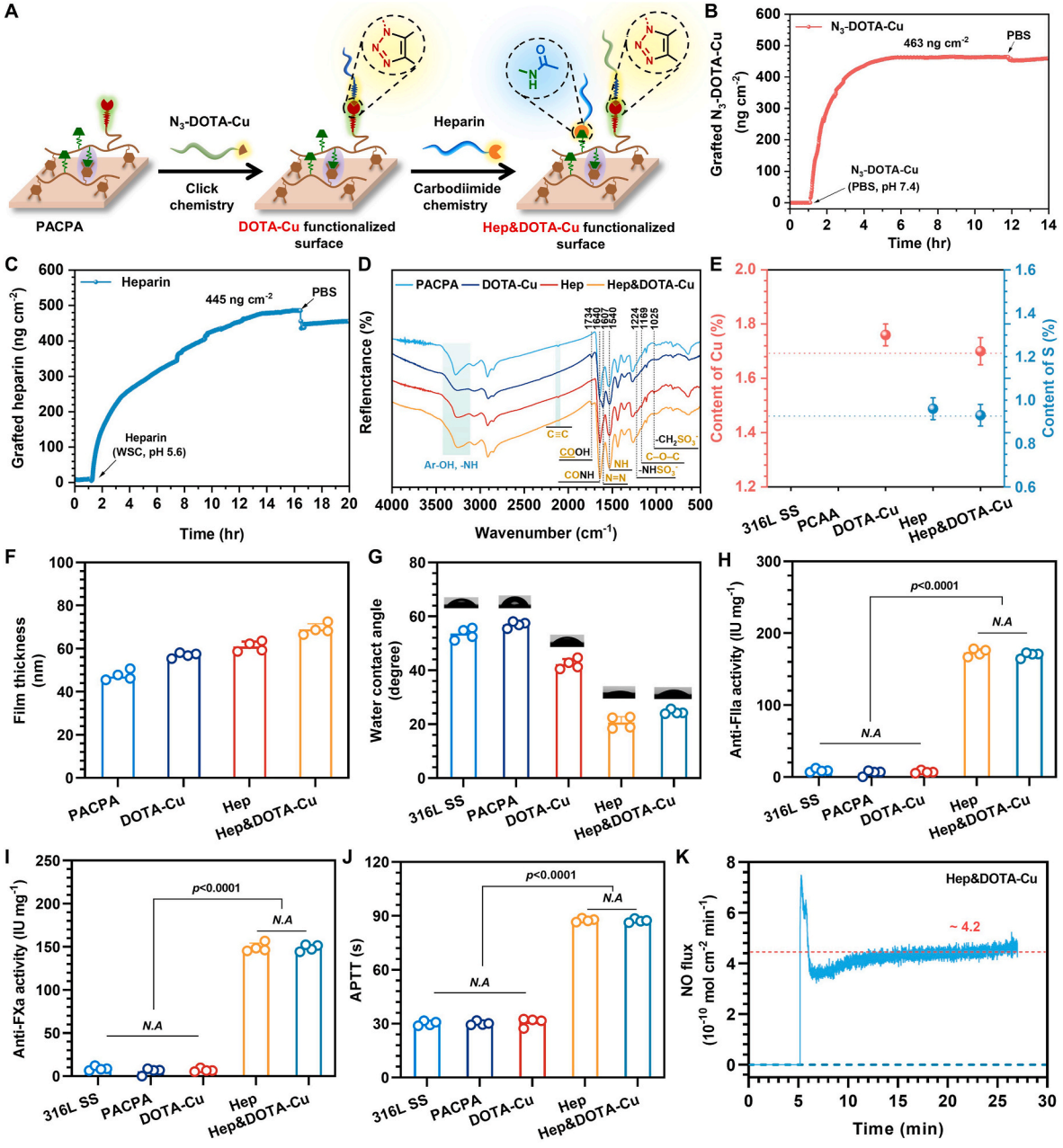

Fig. 3. Preparation and characterization of endothelium-mimicking surfaces. (A) Schematic representation of sequential grafting of N_3-DOTA-Cu and heparin onto the PACPA surface. Real-time QCM-D monitoring of grafting mass for (B) N_3-DOTA-Cu and (C) heparin. (D) FTIR spectra of PACPA, DOTA-Cu, Hep, and Hep&DOTA-Cu surfaces. (E) Cu and S content (%) on 316L SS, PACPA, DOTA-Cu, Hep, and Hep&DOTA-Cu surfaces. (F) Film thickness and (G) WCA of PACPA, DOTA-Cu, Hep, and Hep&DOTA-Cu surfaces. (H) Anti-FIIa activity and (I) anti-FXa activity on the surfaces of 316L SS, PACPA, DOTA-Cu, Hep, and Hep&DOTA-Cu surfaces, along with APTT values (J). (K) Catalytic NO release rate from the Hep&DOTA-Cu coating at 37 °C in PBS. One-way ANOVA followed by Tukey's multiple comparison test was performed to determine the *p*-values as indicated, and $p < 0.05$ suggests a significant difference. *"N.A"* indicates no significant differences between groups. All error bars represent the mean ± SD ($n = 4$).

rapidly immobilized onto the surface, achieving a grafting density of 463 ng cm^{-2} within 2 h (Fig. 3B). In the subsequent heparin grafting, the PACPA coating demonstrated high-efficiency heparin immobilization, maintaining an effective surface density of 445 ng cm^{-2} even after rinsing with PBS (Fig. 3C).

FTIR and XPS analyses were performed to further investigate the chemical structure and composition of the coating. FTIR spectra revealed the disappearance of the -C ≡ C- absorption peak in PACPA after N_3-DOTA-Cu immobilization, accompanied by the emergence of a characteristic triazole ring. This confirms that the azide and alkynyl

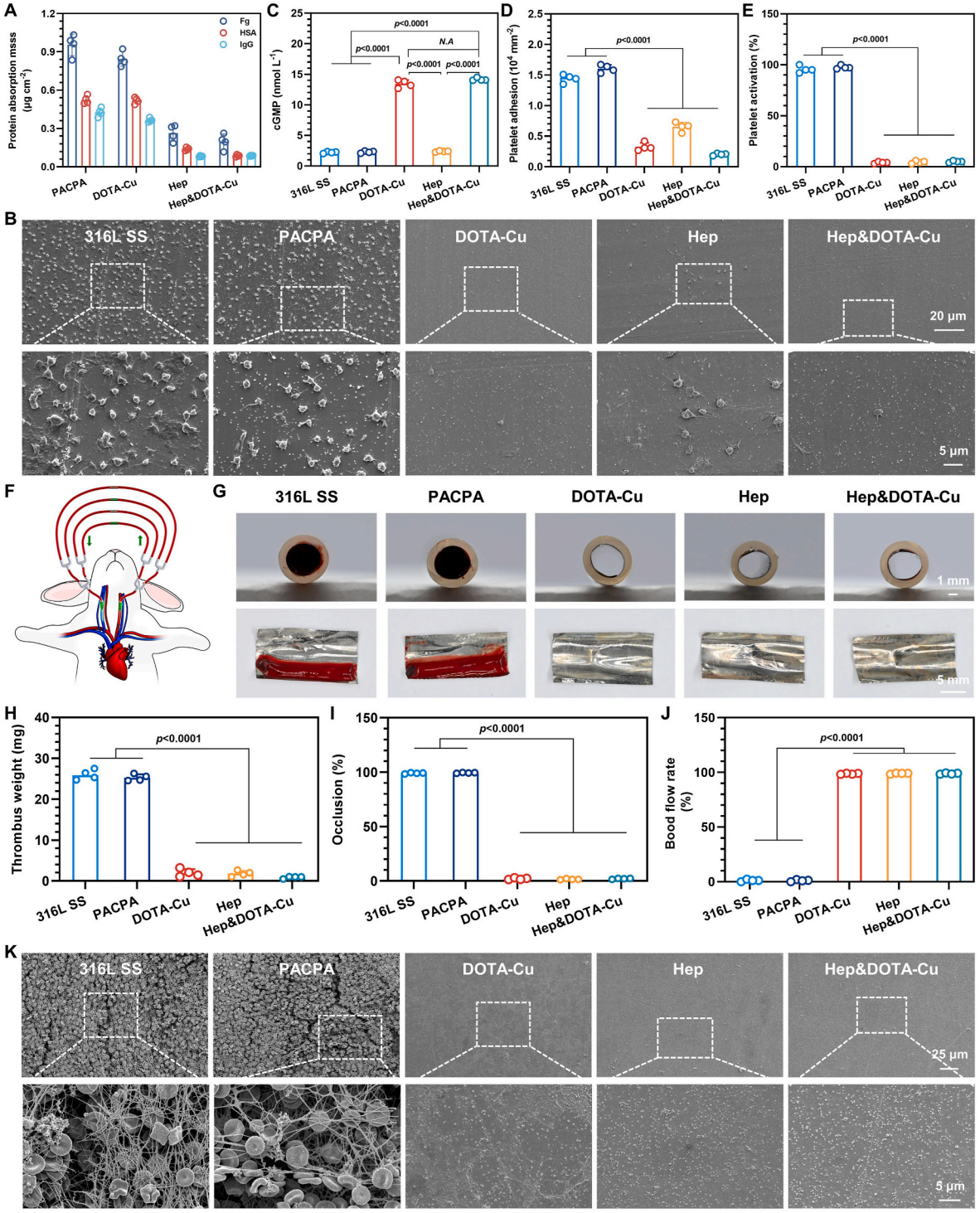

Fig. 4. Evaluation of the antithrombotic properties of endothelial-mimicking surfaces. (A) Adsorbed mass of Fg, HSA, and IgG on PACPA, DOTA-Cu, Hep, and Hep&DOTA-Cu surfaces. (B) Representative SEM images of platelets adhered to different surfaces. (C) Quantitative analysis of cGMP, (D) platelet adhesion and (E) activation (%) after 30 min incubation on different surfaces. (F) Schematic diagram of the New Zealand white rabbit arteriovenous shunt model. (G) Cross-sectional images and photographs of thrombi formed on the surfaces of different samples after 2 h of exposure to anticoagulant-free blood flow. (H) Quantitative evaluation of thrombus weight, (I) occlusion (%), and (J) blood flow rate (%) on different surfaces. (K) Representative SEM images of different surfaces after 2 h of blood circulation. One-way ANOVA followed by Tukey's multiple comparison test was performed to determine the *p*-values as indicated, and $p < 0.05$ suggests a significant difference. "*N.A.*" indicates no significant differences between groups. All error bars represent the mean ± SD ($n = 4$).

groups underwent a highly efficient and specific click chemistry reaction, successfully anchoring N_3-DOTA-Cu onto the PACPA surface [48] (Fig. 3D). After sequential heparin grafting, characteristic FTIR peaks of heparin (-$NHSO_3^-$, -C-O-C-, and -$CH_2SO_3^-$ at 1,224, 1,169, and 1025 cm^{-1} [49,50], respectively) and enhanced amide I and II bands (1640 cm^{-1} and 1540 cm^{-1}) were observed, indicating successful heparin immobilization through condensation reactions with PACPA.

XPS analysis revealed the presence of characteristic Cu and S signals on Hep&DOTA-Cu surface (Fig, 3E and Table S1), further confirming the successful co-immobilization of N_3-DOTA-Cu and heparin. Additionally, the incorporation of these biomolecules increased the coating thickness, indicating that the PACPA surface was completely covered by the NO-generating enzyme and heparin (Fig. 3F). Notably, the abundant hydrophilic groups (sulfonic and carboxylic acid groups) in heparin significantly reduced the WCA on the Hep-PACPA surface to 23.6 ± 2° (Fig. 3G), demonstrating the enhanced wettability of the Hep-functionalized surface. This improved wettability promises better blood compatibility and reduces the adsorption of plasma proteins [51], making the surface highly suitable for blood-contacting devices (Fig. S5). Furthermore, compared to 316 SS, PACPA, and DOTA-Cu, the Hep-functionalized surface (Hep and Hep&DOTA-Cu) significantly reduced the activation of FIIa and FXa (Fig. 3H and I), and prolonged the APTT by over 90 s (Fig. 3J), a change with clinical significance [52]. Importantly, the Hep&DOTA-Cu surface exhibited efficient NO release, with a release rate of 4.2 × 10^{-10} mol cm^{-2} min^{-1} (Fig. 4K), comparable to the natural NO release rate of endothelial cells (0.5–4 × 10^{-10} mol cm^{-2} min^{-1}) and remained unaffected by the subsequent grafting of biomolecules [53]. These results demonstrate that the N_3-DOTA-Cu and heparin were successfully co-grafted onto blood-contacting surfaces via distinct reaction mechanisms, resulting in effective antithrombogenic performance.

3.3. Antithrombotic properties of endothelial-mimicking surfaces

The rapid adsorption of plasma proteins onto the surfaces of blood-contacting devices, resulting in platelet adhesion and activation, is a key initiating event in thrombosis [54]. To evaluate the anti-fouling and platelet-resistant properties of the endothelial-mimicking surfaces, the adsorption of Fg, HSA, and IgG on different surfaces was quantified. As shown in Fig. 4A, PACPA and DOTA-Cu surfaces exhibited relatively high protein adsorption levels (Fg: 955.15 ± 84.12 ng cm^{-2} *vs.* 844.42 ± 57.79 ng cm^{-2}; HSA: 524.28 ± 32.17 ng cm^{-2} *vs.* 518.88 ± 24.41 ng cm^{-2}; IgG: 426.67 ± 33.54 ng cm^{-2} *vs.* 365.25 ± 15.45 ng cm^{-2}). In contrast, the Hep and Hep&DOTA-Cu surfaces significantly reduced protein adsorption (Fg: 265.13 ± 63.78 ng cm^{-2} *vs.* 196.85 ± 60.10 ng cm^{-2}; HSA: 139.40 ± 11.71 ng cm^{-2} *vs.* 86.75 ± 8.06 ng cm^{-2}; IgG: 82.4 ± 4.15 ng cm^{-2} *vs.* 86.82 ± 2.95 ng cm^{-2}). Notably, no significant difference in protein adsorption was observed between Hep and Hep&DOTA-Cu groups. This reduction in protein adsorption can be attributed to the electrostatic interactions between sulfonic acid groups and proteins, along with the enhanced hydrophilicity of the heparin-modified surface [55].

To assess platelet adhesion and activation, the surfaces were exposed to PRP and observed using SEM. On 316L SS and PACPA-coated surfaces, pseudopodia extension was observed (Fig. 4B), indicating high degree of platelet activation [56]. In contrast, DOTA-Cu functionalized surfaces significantly reduced platelet adhesion, and maintained adhered platelets in a spherical, resting state, demonstrating its ability to inhibit platelet adhesion and activation. Similarly, heparin grafting reduced platelet adhesion and aggregation, likely due to the high hydrophilicity and negative charge of the heparinized surface [57]. Moreover, the synergistic effects of NO and heparin further enhanced platelet inhibition. Quantitative analysis revealed that NO coatings significantly suppressed platelet adhesion and activation via cGMP pathway (Fig. 4C–E).

To explore the antithrombogenic performance of endothelial-mimicking surfaces in practical applications, an extracorporeal circulation model was established using New Zealand white rabbits (Fig. 4F). After 2 h of blood circulation, the lumen of 316L SS and PACPA tubes was completely occluded, indicating severe thrombosis. In contrast, DOTA-Cu, Hep and Hep&DOTA-Cu surfaces showed minimal thrombus coverage (Fig. 4G). Quantitative analysis further confirmed that the synergistic effect of DOTA-Cu and heparin (Hep&DOTA-Cu) significantly enhanced antithrombogenic performance compared to 316L SS, as evidenced by a markedly lower thrombus weight (32.61 ± 1.42 mg *vs.* 2.23 ± 0.53 mg, Fig. 4H) and occlusion rate (98.5 ± 1.9 % *vs.* 1.02 ± 0.02 %, Fig. 4I), while maintaining the initial blood flow rate (1.24 ± 0.03 % *vs.* 99.24 ± 1.37 %, Fig. 4J). Representative SEM images illustrated typical thrombus characteristics on the control group surfaces, including platelets and red blood cells embedded within fibrin networks (Fig. 4K). In contrast, Hep&DOTA-Cu surfaces exhibited minimal platelets and plasma proteins, effectively preventing thrombus formation. These results indicate that the dual-functional endothelium-mimetic surface exhibits remarkable antithrombotic performance *in vitro* and *in vivo*.

3.4. Chemical robustness of endothelial-mimicking surfaces

Given the critical importance of stable biomolecules retention on blood-contacting device surfaces for ensuring long-term biological functionality [58,59], we further evaluated the ability of Hep&DOTA-Cu to securely anchor biomolecules under extreme conditions. Specifically, Hep&DOTA-Cu coatings were treated with HCl (pH 2), NaOH (pH 13), or H_2O_2 (0.3 % w/w) for accelerated degradation testing. Representative optical images and SEM micrographs demonstrated no noticeable changes in surface morphology before and after the treatments (Fig. 5A), with no variation in coating thickness or surface hydrophilicity (Fig. 5B and C). Moreover, the chemical composition of the coatings remained largely unaltered, and no reduction in surface Cu or S content was observed (Fig. 5D and Table S2), indicating chemical robustness. Owing to the chemical robustness of the coatings, the catalytic NO release performance also remained stable even after exposure to extreme conditions (Fig. 5E). Furthermore, compared to untreated coatings, the Hep&DOTA-Cu coatings subjected to extreme treatments exhibited no statistically significant changes in suppressing FIIa and FXa activities (Fig. 5F and G), with APTT values remaining consistently stable (Fig. 5H). These results demonstrate the highly chemical robustness of the coating and the highly preserved bioactivity of grafted biomolecules.

Subsequently, we further evaluated the anticoagulant properties of Hep&DOTA-Cu treated with HCl (pH 2), NaOH (pH 13), or H_2O_2 (0.3 % w/w) using anticoagulant-free whole blood. In comparison to the control groups (316L SS and PACPA), the majority of blood on the Hep&DOTA-Cu coated surface remained fluid after 5 min at room temperature, regardless of the treatment (Fig. 5I). This result indicates that the anticoagulant functionality of the Hep&DOTA-Cu coating remains unchanged under extreme environmental conditions. Representative SEM images showed that the control surfaces exhibited typical fibrin networks with entrapped activated platelets and red blood cells. In contrast, the Hep&DOTA-Cu coating demonstrated negligible adhesion of blood cells and reduced plasma proteins adsorption (Fig. 5J). These results demonstrate that the robust endothelium-mimicking coating possesses chemical stability and holds great promise for long-term antithrombotic performance.

3.5. Long-lasting antithrombotic properties of endothelium-mimicking surfaces

Enduring and superior antithrombotic performance is crucial for the long-term service of blood-contacting devices. To evaluate the enduring antithrombotic properties of the endothelium-mimicking surface, Hep&DOTA-Cu coatings were immersed in PBS at 37 °C for varying durations. WCA measurements confirmed that a 4-week immersion did

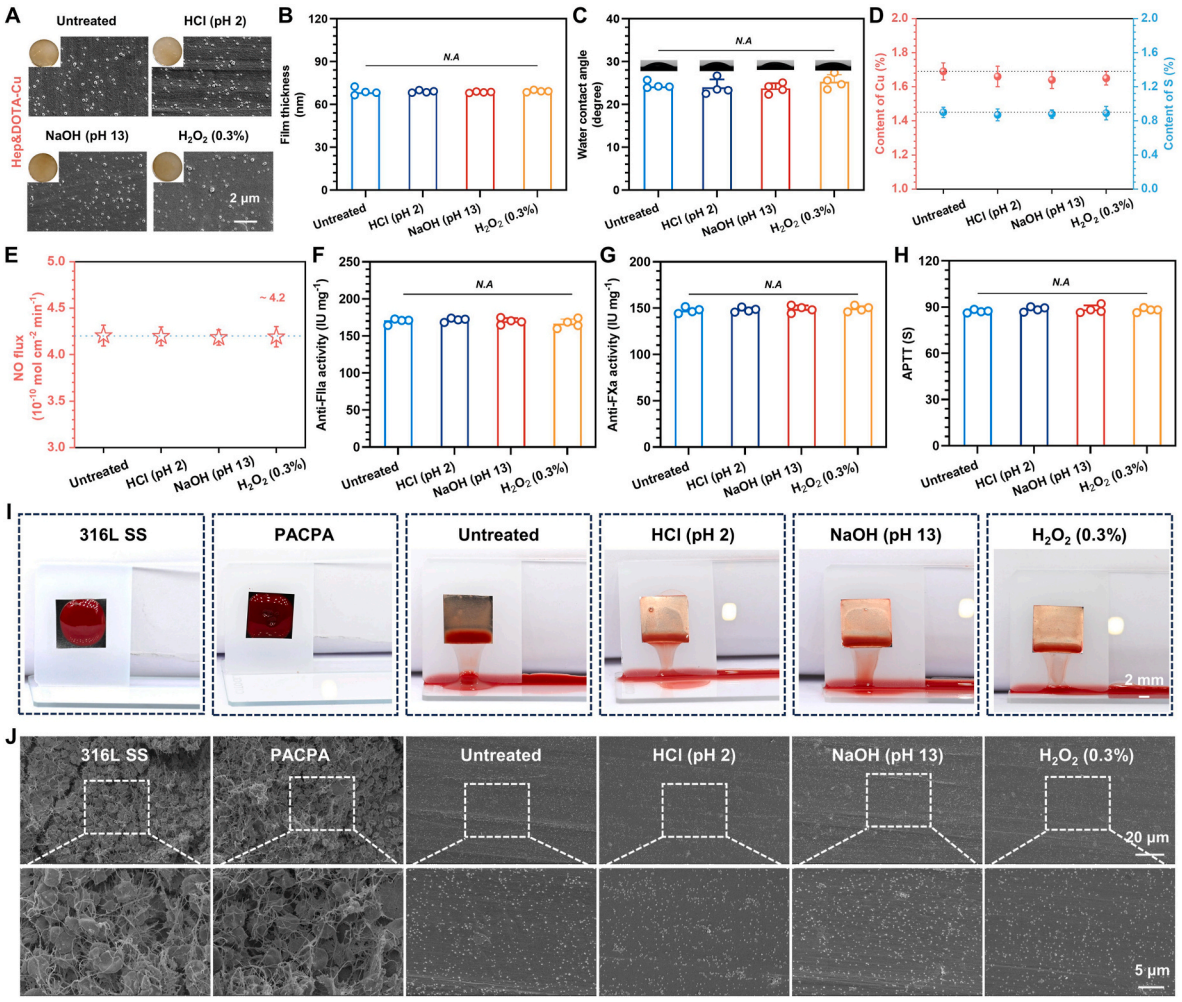

Fig. 5. Evaluation of the chemical robustness of endothelial-mimicking surfaces. (A) Surface photographs and SEM images of Hep&DOTA-Cu coatings before and after 24 h exposure to extreme conditions, including HCl (pH 2), NaOH (pH 13), and H_2O_2 (0.3 % w/w). (B) Film thickness, (C) WCA, and (D) changes in characteristic elements Cu and S of Hep&DOTA-Cu before and after treatment. (E) NO-generation rate, (F) Anti-FIIa, (G) Anti-FXa activities, and (H) APTT values of Hep&DOTA-Cu coatings before and after treatment under extreme conditions. (I) Macroscopic photographs and (J) SEM images of rabbit whole blood after 5 min of static contact with different material surfaces. One-way ANOVA followed by Tukey's multiple comparison test was performed to determine the *p*-values as indicated, and $p < 0.05$ suggests a significant difference. *"N.A."* indicates no significant differences between groups. All error bars represent the mean ± SD ($n = 4$).

not significantly alter the WCA of the Hep&DOTA-Cu surface (Fig. 6A), indicating sustained hydrophilicity and effective suppression of nonspecific protein adsorption. Although slight reductions in surface Cu and S content were observed following immersion, retention levels remained at 85 % of their pre-immersion values (Fig. 6B), respectively, demonstrating chemical stability and robust biomolecule anchoring. Furthermore, owing to the chemical robustness of the PACPA coating, Hep&DOTA-Cu retained its superior NO generation capacity and coagulation factor inhibition. Even after 4 weeks of immersion, the catalytic NO release rate remained as high as 88 % (Fig. 6C), while anti-FIIa and -FXa activity retention rates exceeded 86 % (Fig. 6D).

To further validate the long-term antithrombotic performance of Hep&DOTA-Cu, *ex vivo* circulation experiments were conducted. After 2 h of blood circulation, severe thrombosis was observed on the control surfaces (316L SS and PACPA), whereas Hep&DOTA-Cu-coated 316L SS exhibited almost no thrombosis, even after 4 weeks of immersion (Fig. 6E). Quantitative analysis revealed that Hep&DOTA-Cu significantly reduced thrombus weight (Fig. 6F), and occlusion rate (Fig. 6G), with the blood flow rates maintaining over 95 % (Fig. 6H). Representative SEM images further demonstrated minimal blood cell adhesion on the Hep&DOTA-Cu surface, both before and after immersion, in stark contrast to the control surfaces (Fig. 6I). These results confirm that the endothelium-mimicking coating maintains long-lasting antithrombogenic efficacy, thereby meeting the critical requirements for long-term functionality in blood-contacting medical devices/materials.

4. Conclusions

In this study, we developed endothelium-mimicking coatings with enduring and superior antithrombotic properties using dual-biomimetic surface chemistry strategies. The long-acting endothelium-mimicking antithrombotic coatings, which were firstly pre-coated by a chemically robust coating using a Mefp-5 mimic bearing amine, phenolic hydroxyl and clickable alkynyl groups, followed by sequential co-immobilization of heparin and clickable NO-generating enzyme (N_3-DOTA-Cu) via carbodiimide and click chemistry, respectively. Owing to the exceptional chemical stability of the pre-coatings and the robust covalent anchoring of target molecules, the endothelium-mimicking coatings we developed demonstrated a high heparin bioactivity retention rate of 86 % and NO catalytic efficiency of 88 % after 4 weeks of PBS treatment. Consequently, the coatings showed enduring and superior anticoagulant and anti-platelet properties *in vitro* and non-thrombogenic properties *in vivo*, similar to natural endothelium. We believe that this endothelium-mimicking antithrombotic coating represents a promising

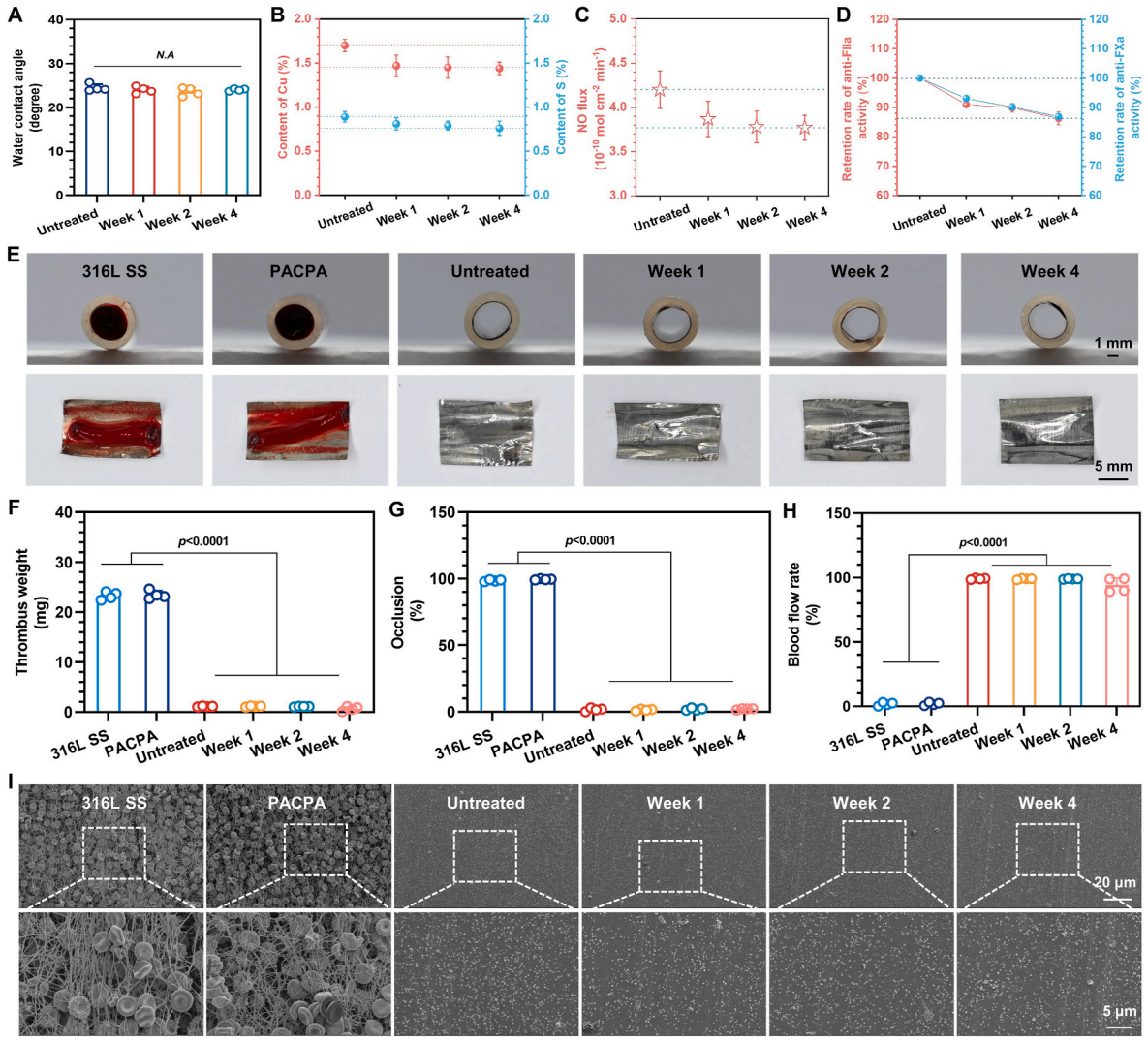

Fig. 6. Evaluation of enduring anti-thrombotic properties of endothelium-mimicking surfaces. (A) WCA, (B) content of Cu and S (%), (C) NO catalytic release rate, (D) retention rate of anti-FIIa and -FXa activity of Hep&DOTA-Cu before and after immersion in PBS for 1 week, 2 weeks, and 4 weeks, respectively. (E) Cross-section (upper row) and surface thrombus (lower row) of catheters installed with different samples after 2 h of blood circulation. (F) Quantitative results of thrombus weight on the surfaces of different samples. (G) Occlusion rate (%) of catheters loaded with different samples after 2 h of blood circulation. (H) Blood flow rates (%) of catheters loaded with different samples. (I) Representative SEM images of thrombus on the surfaces of different samples. One-way ANOVA followed by Tukey's multiple comparison test was performed to determine the *p*-values as indicated, and $p < 0.05$ suggests a significant difference. *"N.A."* indicates no significant differences between groups. All error bars represent the mean ± SD ($n = 4$).

functional platform for addressing antithrombotic challenges in blood-contacting devices.

CRediT authorship contribution statement

Zeyu Du: Writing – original draft, Validation, Methodology, Investigation, Data curation. **Yuting Huang:** Data curation, Methodology. **Qing Ma:** Writing – review & editing, Methodology. **Wentai Zhang:** Writing – review & editing, Methodology. **Yan Fu:** Writing – review & editing, Methodology. **Nan Huang:** Methodology, Funding acquisition. **Xin Li:** Project administration, Funding acquisition. **Zhilu Yang:** Writing – review & editing, Supervision, Project administration, Funding acquisition. **Wenjie Tian:** Project administration, Funding acquisition.

Ethics approval and consent to participate

All animal experiments adhered to the Laboratory Animal Administration Rules of China and were approved by the Dongguan People's Hospital Laboratory Animal Welfare and Ethics Committee (Approval No.: IACUC-AWEC-202405502).

Data availability statement

The data that support the findings of this study are available from the corresponding author upon reasonable request.

Declaration of competing interest

The authors declare the following personal relationships which may be considered as potential competing interests: Nan Huang is currently employed by GuangZhou Nanchuang Mount Everest Company for Medical Science and Technology.

Acknowledgments

Natural Science Foundation of China (Project 32371377, 32171326, 82470532, 32471376, 32371378, 32261160372), The Third People's

Hospital of Chengdu Scientific Research Project (2023PI11), the Guang Dong Basic and Applied Basic Research Foundation (2022B1515130010), Dongguan Science and Technology of Social Development Program (20231800906311), and the Leading Talent Project of Guangzhou Development District (2020-L013). We would like to thank the Analytical and Testing Centerfor their support.

Supplementary data

Supplementary data to this article can be found online at https://doi.org/10.1016/j.bioactmat.2025.03.019.

References

[1] X. Wang, M. Yu, M. Kamal Hadi, J. Niu, Y. Zhang, Q. Zhou, F. Ran, An anticoagulant supercapacitor for implantable applications, Nat. Commun. 15 (2024) 10497, https://doi.org/10.1038/s41467-024-54862-2.
[2] A. Khan, R. Joshi, M.K. Sharma, A. Ganguly, P. Parashar, T.-W. Wang, S. Lee, F.-C. Kao, Z.-H. Lin, Piezoelectric and triboelectric nanogenerators: promising technologies for self-powered implantable biomedical devices, Nano Energy 119 (2024) 109051, https://doi.org/10.1016/j.nanoen.2023.109051.
[3] M.H. Yacoub, C. McLeod, The expanding role of implantable devices to monitor heart failure and pulmonary hypertension, Nat. Rev. Cardiol. 15 (2018) 770–779, https://doi.org/10.1038/s41569-018-0103-z.
[4] Y.J. Hong, H. Jeong, K.W. Cho, N. Lu, D. Kim, Wearable and implantable devices for cardiovascular healthcare: from monitoring to therapy based on flexible and stretchable electronics, Adv. Funct. Mater. 29 (2019) 1808247, https://doi.org/10.1002/adfm.201808247.
[5] Z. Dou, S. Chen, J. Wang, L. Xia, M.F. Maitz, Q. Tu, W. Zhang, Z. Yang, N. Huang, A "built-up" composite film with synergistic functionalities on Mg-2Zn-1Mn bioresorbable stents improves corrosion control effects and biocompatibility, Bioact. Mater. 25 (2023) 223–238, https://doi.org/10.1016/j.bioactmat.2023.02.004.
[6] D. Gailani, A. Gruber, Targeting factor XI and factor XIa to prevent thrombosis, Blood 143 (2024) 1465–1475, https://doi.org/10.1182/blood.2023020722.
[7] B.P. Nguyen Thi, B.T. Duy Nguyen, I.-S. Jeong, J.F. Kim, Hemocompatibility challenge of membrane oxygenator for artificial lung technology, Acta Biomater. 152 (2022) 19–46, https://doi.org/10.1016/j.actbio.2022.09.003.
[8] A.M. Wendelboe, G.E. Raskob, Global burden of thrombosis, Circ. Res. 118 (2016) 1340–1347, https://doi.org/10.1161/CIRCRESAHA.115.306841.
[9] E.E. Moore, H.B. Moore, L.Z. Kornblith, M.D. Neal, M. Hoffman, N.J. Mutch, H. Schöchl, B.J. Hunt, A. Sauaia, Trauma-induced coagulopathy, Nat. Rev. Dis. Primers 7 (2021) 30, https://doi.org/10.1038/s41572-021-00264-3.
[10] J. Thomas, V. Kostousov, J. Teruya, Bleeding and thrombotic complications in the use of extracorporeal membrane oxygenation, Semin. Thromb. Hemost. 44 (2018) 20–29, https://doi.org/10.1055/s-0037-1606179.
[11] J.I. Weitz, J. Harenberg, New developments in anticoagulants: past, present and future, Thromb. Haemost. 117 (2017) 1283–1288, https://doi.org/10.1160/TH16-10-0807.
[12] A. Mangieri, C. Montalto, E. Poletti, A. Sticchi, G. Crimi, F. Giannini, A. Latib, D. Capodanno, A. Colombo, Thrombotic versus bleeding risk after transcatheter aortic valve replacement, J. Am. Coll. Cardiol. 74 (2019) 2088–2101, https://doi.org/10.1016/j.jacc.2019.08.1032.
[13] Q. Tu, X. Shen, Y. Liu, Q. Zhang, X. Zhao, M.F. Maitz, T. Liu, H. Qiu, J. Wang, N. Huang, Z. Yang, A facile metal-phenolic-amine strategy for dual-functionalization of blood-contacting devices with antibacterial and anticoagulant properties, Mater. Chem. Front. 3 (2019) 265–275, https://doi.org/10.1039/C8QM00458G.
[14] T. Bakchoul, I. Marini, Drug-associated thrombocytopenia, Hematol. Am. Soc. Hematol. Educ. Program 2018 (2018) 576–583, https://doi.org/10.1182/asheducation-2018.1.576.
[15] A. Qamar, M. Vaduganathan, N.J. Greenberger, R.P. Giugliano, Oral anticoagulation in patients with liver disease, J. Am. Coll. Cardiol. 71 (2018) 2162–2175, https://doi.org/10.1016/j.jacc.2018.03.023.
[16] H. Al-Samkari, J.M. Connors, Managing the competing risks of thrombosis, bleeding, and anticoagulation in patients with malignancy, Hematology 2019 (2019) 71–79, https://doi.org/10.1182/hematology.2019000369.
[17] C. Sperling, M. Fischer, M.F. Maitz, C. Werner, Blood coagulation on biomaterials requires the combination of distinct activation processes, Biomaterials 30 (2009) 4447–4456, https://doi.org/10.1016/j.biomaterials.2009.05.044.
[18] B. Estevez, X. Du, New concepts and mechanisms of platelet activation signaling, Physiology 32 (2017) 162–177, https://doi.org/10.1152/physiol.00020.2016.
[19] J. Li, K. Zhang, N. Huang, Engineering cardiovascular implant surfaces to create a vascular endothelial growth microenvironment, Biotechnol. J. 12 (2017) 1600401, https://doi.org/10.1002/biot.201600401.
[20] S.J. Lee, H.H. Jo, K.S. Lim, D. Lim, S. Lee, J.H. Lee, W.D. Kim, M.H. Jeong, J.Y. Lim, I.K. Kwon, Y. Jung, J.-K. Park, S.A. Park, Heparin coating on 3D printed poly (l-lactic acid) biodegradable cardiovascular stent via mild surface modification approach for coronary artery implantation, Chem. Eng. J. 378 (2019) 122116, https://doi.org/10.1016/j.cej.2019.122116.
[21] X. Mou, W. Miao, W. Zhang, W. Wang, Q. Ma, Z. Du, X. Li, N. Huang, Z. Yang, Zwitterionic polymers-armored amyloid-like protein surface combats thrombosis and biofouling, Bioact. Mater. 32 (2024) 37–51, https://doi.org/10.1016/j.bioactmat.2023.09.003.
[22] W.J. Geelhoed, K.E.A. Van Der Bogt, T.C. Rothuizen, F.F.R. Damanik, J. F. Hamming, C.D. Mota, M.S. Van Agen, H.C. De Boer, M.T. Restrepo, B. Hinz, A. Kislaya, C. Poelma, A.J. Van Zonneveld, T.J. Rabelink, L. Moroni, J.I. Rotmans, A novel method for engineering autologous non-thrombogenic in situ tissue-engineered blood vessels for arteriovenous grafting, Biomaterials 229 (2020) 119577, https://doi.org/10.1016/j.biomaterials.2019.119577.
[23] I. Adipurnama, M.-C. Yang, T. Ciach, B. Butruk-Raszeja, Surface modification and endothelialization of polyurethane for vascular tissue engineering applications: a review, Biomater. Sci. 5 (2017) 22–37, https://doi.org/10.1039/C6BM00618C.
[24] D. Radke, W. Jia, D. Sharma, K. Fena, G. Wang, J. Goldman, F. Zhao, Tissue engineering at the blood-contacting surface: a review of challenges and strategies in vascular graft development, Adv. Healthcare Mater. 7 (2018) 1701461, https://doi.org/10.1002/adhm.201701461.
[25] Y. Wang, H. Wu, Z. Zhou, M.F. Maitz, K. Liu, B. Zhang, L. Yang, R. Luo, Y. Wang, A thrombin-triggered self-regulating anticoagulant strategy combined with anti-inflammatory capacity for blood-contacting implants, Sci. Adv. 8 (2022) eabm3378, https://doi.org/10.1126/sciadv.abm3378.
[26] A. Krüger-Genge, A. Blocki, R.-P. Franke, F. Jung, Vascular endothelial cell biology: an update, Int. J. Mol. Sci. 20 (2019) 4411, https://doi.org/10.3390/ijms20184411.
[27] B. Yi, B. Zhou, Z. Song, L. Yu, W. Wang, W. Liu, Step-wise CAG@PLys@PDA-Cu^{2+} modification on micropatterned nanofibers for programmed endothelial healing, Bioact. Mater. 25 (2023) 657–676, https://doi.org/10.1016/j.bioactmat.2022.07.010.
[28] M.F. Maitz, J. Zitzmann, J. Hanke, C. Renneberg, M.V. Tsurkan, C. Sperling, U. Freudenberg, C. Werner, Adaptive release of heparin from anticoagulant hydrogels triggered by different blood coagulation factors, Biomaterials 135 (2017) 53–61, https://doi.org/10.1016/j.biomaterials.2017.04.044.
[29] J. Li, B. Jiang, X. Chang, H. Yu, Y. Han, F. Zhang, Bi-terminal fusion of intrinsically-disordered mussel foot protein fragments boosts mechanical strength for protein fibers, Nat. Commun. 14 (2023) 2127, https://doi.org/10.1038/s41467-023-37563-0.
[30] Z. Du, F. Qiao, L. Tong, W. Zhang, X. Mou, X. Zhao, M.F. Maitz, H. Wang, N. Huang, Z. Yang, Mimicking Mytilus edulis foot protein: a versatile strategy for robust biomedical coatings, Innovation 5 (2024) 100671, https://doi.org/10.1016/j.xinn.2024.100671.
[31] M.L. Alfieri, T. Weil, D.Y.W. Ng, V. Ball, Polydopamine at biological interfaces, Adv. Colloid Interface Sci. 305 (2022) 102689, https://doi.org/10.1016/j.cis.2022.102689.
[32] J. Chen, Q. Peng, X. Peng, H. Zhang, H. Zeng, Probing and manipulating noncovalent interactions in functional polymeric systems, Chem. Rev. 122 (2022) 14594–14678, https://doi.org/10.1021/acs.chemrev.2c00215.
[33] M.A. Gebbie, W. Wei, A.M. Schrader, T.R. Cristiani, H.A. Dobbs, M. Idso, B. F. Chmelka, J.H. Waite, J.N. Israelachvili, Tuning underwater adhesion with cation–π interactions, Nat. Chem. 9 (2017) 473–479, https://doi.org/10.1038/nchem.2720.
[34] P. Gao, H. Qiu, K. Xiong, X. Li, Q. Tu, H. Wang, N. Lyu, X. Chen, N. Huang, Z. Yang, Metal-catechol-(amine) networks for surface synergistic catalytic modification: therapeutic gas generation and biomolecule grafting, Biomaterials 248 (2020) 119981, https://doi.org/10.1016/j.biomaterials.2020.119981.
[35] W. Wang, Q. Ma, D. Li, W. Zhang, Z. Yang, W. Tian, N. Huang, Engineered endothelium-mimicking antithrombotic surfaces via combination of nitric oxide-generation with fibrinolysis strategies, Bioact. Mater. 43 (2025) 319–329, https://doi.org/10.1016/j.bioactmat.2024.09.011.
[36] M. Patel, S. Mestry, G. Phalak, S. Mhaske, Novel catechol-derived phosphorus-based precursors for coating applications, Polym. Bull. 77 (2020) 2183–2203, https://doi.org/10.1007/s00289-019-02855-3.
[37] L.A. Brandner, B. Marmiroli, M. Linares-Moreau, M. Barella, B. Abbasgholi-Na, M. D.J. Velásquez-Hernández, K.L. Flint, S. Dal Zilio, G.P. Acuna, H. Wolinski, H. Amenitsch, C.J. Doonan, P. Falcaro, Ordered transfer from 3D-oriented MOF superstructures to polymeric films: microfabrication, enhanced chemical stability, and anisotropic fluorescent patterns, Adv. Mater. 36 (2024) 2404384, https://doi.org/10.1002/adma.202404384.
[38] C. Hu, H. Wei, B. Hua, Y. Zhang, G. Wang, T. Guo, Facile fabrication of a broad-spectrum starch/poly(α-l-lysine) hydrogel adsorbent with thermal/pH-sensitive IPN structure through simultaneous dual-click strategy, Carbohydr. Polym. 309 (2023) 120672, https://doi.org/10.1016/j.carbpol.2023.120672.
[39] H. Qiu, P. Qi, J. Liu, Y. Yang, X. Tan, Y. Xiao, M.F. Maitz, N. Huang, Z. Yang, Biomimetic engineering endothelium-like coating on cardiovascular stent through heparin and nitric oxide-generating compound synergistic modification strategy, Biomaterials 207 (2019) 10–22, https://doi.org/10.1016/j.biomaterials.2019.03.033.
[40] A. Schwaighofer, M. Montemurro, S. Freitag, C. Kristament, M.J. Culzoni, B. Lendl, Beyond fourier transform infrared spectroscopy: external cavity quantum cascade laser-based mid-infrared transmission spectroscopy of proteins in the amide I and amide II region, Anal. Chem. 90 (2018) 7072–7079, https://doi.org/10.1021/acs.analchem.8b01632.
[41] M.J.K. Lodhi, K.M. Deen, M.C. Greenlee-Wacker, W. Haider, Additively manufactured 316L stainless steel with improved corrosion resistance and biological response for biomedical applications, Addit. Manuf. 27 (2019) 8–19, https://doi.org/10.1016/j.addma.2019.02.005.
[42] T. Hu, C. Yang, S. Lin, Q. Yu, G. Wang, Biodegradable stents for coronary artery disease treatment: recent advances and future perspectives, Mater. Sci. Eng. C 91 (2018) 163–178, https://doi.org/10.1016/j.msec.2018.04.100.

[43] B. Li, D. Ni, J. Fan, J. Zhou, Vapor phase polymerized high-performance Poly(3,4-ethylenedioxythiophene) using polyethyleneimine (PEI) as the base inhibitor and grafting agent for electrochromic medical face shields, Chem. Eng. J. 445 (2022) 136818, https://doi.org/10.1016/j.cej.2022.136818.
[44] Z. Hu, R.M. Berry, R. Pelton, E.D. Cranston, One-pot water-based hydrophobic surface modification of cellulose nanocrystals using plant polyphenols, ACS Sustain. Chem. Eng. 5 (2017) 5018–5026, https://doi.org/10.1021/acssuschemeng.7b00415.
[45] S. Wu, J. Xu, L. Zou, S. Luo, R. Yao, B. Zheng, G. Liang, D. Wu, Y. Li, Long-lasting renewable antibacterial porous polymeric coatings enable titanium biomaterials to prevent and treat peri-implant infection, Nat. Commun. 12 (2021) 3303, https://doi.org/10.1038/s41467-021-23069-0.
[46] Z. Huang, H. Ghasemi, Hydrophilic polymer-based anti-biofouling coatings: preparation, mechanism, and durability, Adv. Colloid Interface Sci. 284 (2020) 102264, https://doi.org/10.1016/j.cis.2020.102264.
[47] X. Mou, H. Zhang, H. Qiu, W. Zhang, Y. Wang, K. Xiong, N. Huang, H.A. Santos, Z. Yang, Mussel-Inspired and Bioclickable Peptide Engineered Surface to Combat Thrombosis and Infection, Research 2022 (2022) 2022/9780879. doi:10.34133/2022/9780879.
[48] Y. Xiao, W. Wang, X. Tian, X. Tan, T. Yang, P. Gao, K. Xiong, Q. Tu, M. Wang, M.F. Maitz, N. Huang, G. Pan, Z. Yang, A Versatile Surface Bioengineering Strategy Based on Mussel-Inspired and Bioclickable Peptide Mimic, Research 2020 (2020) 2020/7236946. doi:10.34133/2020/7236946.
[49] M. Tang, J. Xue, K. Yan, T. Xiang, S. Sun, C. Zhao, Heparin-like surface modification of polyethersulfone membrane and its biocompatibility, J. Colloid Interface Sci. 386 (2012) 428–440, https://doi.org/10.1016/j.jcis.2012.07.076.
[50] Y. Liu, Q. Han, T. Li, J. Hua, F. Liu, Q. Li, G. Deng, Heparin reduced dialysis through a facile anti-coagulant coating on flat and hollow fiber membranes, J. Membr. Sci. 595 (2020) 117593, https://doi.org/10.1016/j.memsci.2019.117593.
[51] M.F. Maitz, M.C.L. Martins, N. Grabow, C. Matschegewski, N. Huang, E.L. Chaikof, M.A. Barbosa, C. Werner, C. Sperling, The blood compatibility challenge. Part 4: surface modification for hemocompatible materials: passive and active approaches to guide blood-material interactions, Acta Biomater. 94 (2019) 33–43, https://doi.org/10.1016/j.actbio.2019.06.019.
[52] J. Hirsh, S.S. Anand, J.L. Halperin, V. Fuster, Guide to anticoagulant therapy: heparin: A statement for healthcare professionals from the American heart association, Circulation 103 (2001) 2994–3018, https://doi.org/10.1161/01.CIR.103.24.2994.
[53] Z. Yang, Y. Yang, K. Xiong, X. Li, P. Qi, Q. Tu, F. Jing, Y. Weng, J. Wang, N. Huang, Nitric oxide producing coating mimicking endothelium function for multifunctional vascular stents, Biomaterials 63 (2015) 80–92, https://doi.org/10.1016/j.biomaterials.2015.06.016.
[54] J.L. Brash, T.A. Horbett, R.A. Latour, P. Tengvall, The blood compatibility challenge. Part 2: protein adsorption phenomena governing blood reactivity, Acta Biomater. 94 (2019) 11–24, https://doi.org/10.1016/j.actbio.2019.06.022.
[55] S. Gupta, Y.M. Puttaiahgowda, L. Deiglmayr, Recent advances in the design and immobilization of heparin for biomedical application: a review, Int. J. Biol. Macromol. 264 (2024) 130743, https://doi.org/10.1016/j.ijbiomac.2024.130743.
[56] P.E.J. Van Der Meijden, J.W.M. Heemskerk, Platelet biology and functions: new concepts and clinical perspectives, Nat. Rev. Cardiol. 16 (2019) 166–179, https://doi.org/10.1038/s41569-018-0110-0.
[57] Y. Zhang, L. Zhang, S. Duan, Y. Hu, X. Ding, Y. Zhang, Y. Li, Y. Wu, X. Ding, F.-J. Xu, Heparinized anticoagulant coatings based on polyphenol-amine inspired chemistry for blood-contacting catheters, J. Mater. Chem. B 10 (2022) 1795–1804, https://doi.org/10.1039/D1TB02582A.
[58] J. Cui, S. Jia, Organic–inorganic hybrid nanoflowers: a novel host platform for immobilizing biomolecules, Coord. Chem. Rev. 352 (2017) 249–263, https://doi.org/10.1016/j.ccr.2017.09.008.
[59] D.M. Mitrea, M. Mittasch, B.F. Gomes, I.A. Klein, M.A. Murcko, Modulating biomolecular condensates: a novel approach to drug discovery, Nat. Rev. Drug Discov. 21 (2022) 841–862, https://doi.org/10.1038/s41573-022-00505-4.